Silicon Photonics Programmable Millimeter-Wave Band RF Synthesizer

Claudio Porzi[1], Antonio Malacarne[(2)], Alessandra Bigongiari[(3)], Antonio D'Errico[(3)], Antonella Bogoni[(1,2)]

[(1)] TeCIP Institute, Scuola Superiore Sant'Anna, Pisa, Italy, claudio.porzi@santannapisa.it.
[(2)] Photonic Networks & Technologies National Laboratory, CNIT, Pisa, Italy.
[(3)] Ericsson Research, Pisa, Italy.

Abstract *Using an on-chip optical frequency comb source and advanced optical filters, flexible generation of stable RF carriers in the millimeter-wave band is realized in silicon on insulator technology. Preliminary characterization demonstrates up to tenfold multiplication of a reference local oscillator signal at 20 GHz.*

Introduction

The use of carrier frequencies in the millimeter wave band (i.e., between 30 and 300 GHz) in RF systems has been subject of intense investigation in the last decade. Over this broad range of frequencies, a variety of advanced applications have indeed been identified, including broadband low latency services and wireless backhauling for 5G/6G mobile networks, short-range radar, and THz imaging [1-4]. With respect to standard BiCMOS-based solutions [5], microwave photonics permits flexible generation of arbitrary large carrier frequencies and offers advantages such as widely reconfigurable operation and efficient distribution of the RF signals over low-loss and EMI-free fiber-optic links [6-8]. System miniaturization through a suitable integration technology is regarded as a further step for making photonics-based RF synthesizers a viable alternative to electronics devices, therefore enabling its exploitation in several practical environments [9-12].

We recently reported of programmable and low phase noise RF generation up the W-band with a photonic integrated circuit (PIC) in silicon on insulator (SOI) technology [12]. Here, a novel scheme further extending the range of generated frequencies is presented and characterized.

Operation and circuit implementation

The schematic operation of the proposed programmable frequency multiplier is shown in Fig. 1(a). The light from an external laser source at the optical frequency ν_0 is injected into the PIC and delivered to an optical frequency comb (OFC) source driven by a local oscillator (LO) signal at f_{LO}. An optical splitter (OS) separates the OFC signal into two paths, each comprising a tunable optical filter (OF) isolating a single harmonic from the comb spectrum. The outputs of the OFs are then recombined through an optical coupler (OC). Assuming the OF1 central frequency ν_{OF1} is set at $\nu_0 + n \cdot f_{LO}$, and that of OF2 is $\nu_{OF2} = \nu_0 - m \cdot f_{LO}$, being n and m integers, two optical tones spaced by $(m+n) \cdot f_{LO}$ are produced the PIC output. A high-speed photodiode (PD), after an optional optical link, can then be used to generate a frequency-multiplied version of the LO carrier. Programmable RF synthesis operation is enabled with proper choice of f_{LO} and of the selected harmonic orders m and n.

The generated mask layout for circuit realization in SOI technology using a multi-project wafer service [13] is also shown in Fig. 2(b). Two different OFC sources have been independently connected to each of the input ports of the 2 × 2 OS before the filters' paths. The OFC1 source is

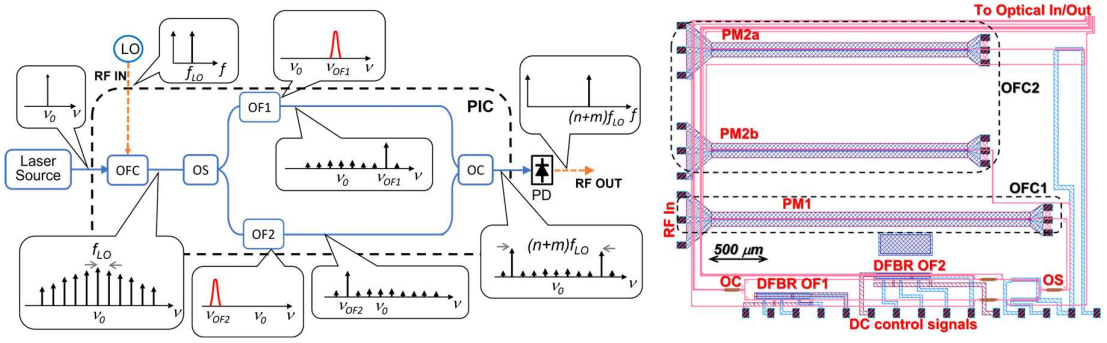

(a) (b)

Fig. 1: (a) Schematic operation of the reconfigurable millimeter wave-band RF carrier synthesizer; (b) Mask layout for circuit realization in silicon on insulator technology.

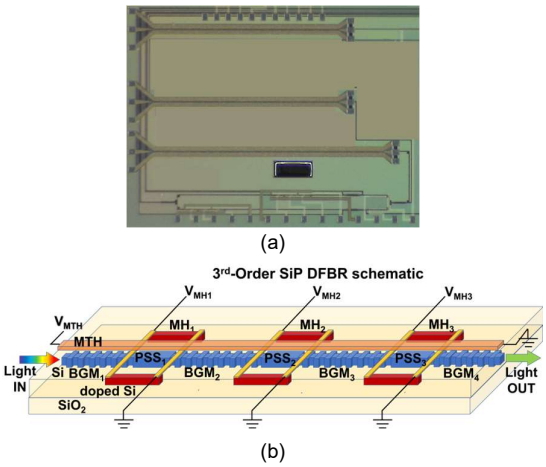

Fig. 2: (a) Picture of fabricated device; (b) Schematic structure of a 3rd-order DFBR silicon photonics filter.

simply based on a single 2 mm-long silicon photonics (SiP) phase modulator (PM1), whereas the other OFC2 source comprises a cascade of the two 1.5 mm-long PM2a and PM2b. The integrated OFs are implemented with third-order distributed feedback resonator (DFBR) structures based on waveguide Bragg gratings [14]. The overall footprint of the circuit (considering only the single PM1-based OFC source) is less than 3.5 mm^2. A micrograph of a fabricated sample is also shown in Fig. 2(a). By including on-chip OFC generation and advanced OFs design, the circuit refines the preliminary work reported in [11].

Integrated filters characterization

The schematic structure of the 3rd-order DFBR filter is shown in Fig. 2(b). Three coupled cavities realized by embedding phase shift sections (PSSs) between four distributed Bragg grating mirrors (BGMs) create a passband transmission window within the mirrors' reflection band. For the sake of simply setting the relative detuning of the central frequency for the two OFs, the devices

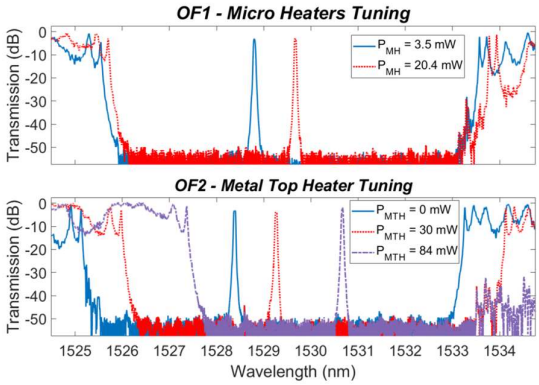

Fig. 3: Tuning of the DFBR optical filters through either local micro heaters (MHs) acting on individual cavities (top traces) or shifting the Bragg wavelength of the distributed mirrors with metal top heater (MTH, bottom traces).

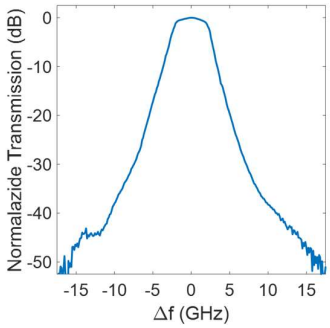

Fig. 4: Derails of the silicon photonics DFBR OFs passband around central frequency.

encompass two different tuning mechanisms. As illustrated in Fig. 2(b), each PSS can be individually controlled by means of three pairs of doped-silicon local micro heaters (MHs), symmetrically placed at the sides of the silicon waveguide. Acting on the optical paths of the distributed cavities is effective for counteracting fabrication imperfections and reconstructing the ideal filter shape in fabricated devices, and additionally permits tuning of the passband central frequency without affecting the edges of stopband region. This is illustrated in the top trace of Fig. 3, where two different tuning of the passband within an 8 nm-wide stopband region, for two levels of the overall power absorbed by the MHs, P_{MH}, are reported. The slight shift of the stopband edges, due to residual thermal leakage toward the BGMs, can be mitigated with optimized MHs position and geometry.

A second metal top heater (MTH) over the whole DFBR structure is additionally placed above the oxide cladding covering the silicon waveguides. The effect of the MTH is to induce a red shift of the Bragg wavelength of the distributed mirrors, and conversely provide a rigid translation of the whole resonator transmission spectrum. This is illustrated in the bottom plots of Fig. 3 for three different values of the dissipated power from the MTH, P_{MTH}. As shown, the combined action of the two tuning mechanisms together with the wide OFs stopband, allows OFC tones spaced by hundreds of GHz to be independently processed with moderate insertion loss of about 2.5 dB.

Finally, the details of the typical transmission peak for the two identical OFs are illustrated in Fig. 4. A flat-top passband with a -1 dB width of about 4 GHz, and a rejection of 40 dB at 10 GHz away from the central frequency which becomes as large as 50 dB above 15 GHz, are measured.

RF synthesis operation

A preliminary characterization of the proposed silicon photonics RF synthesizer is performed by considering the simple single PM1-based OFC1

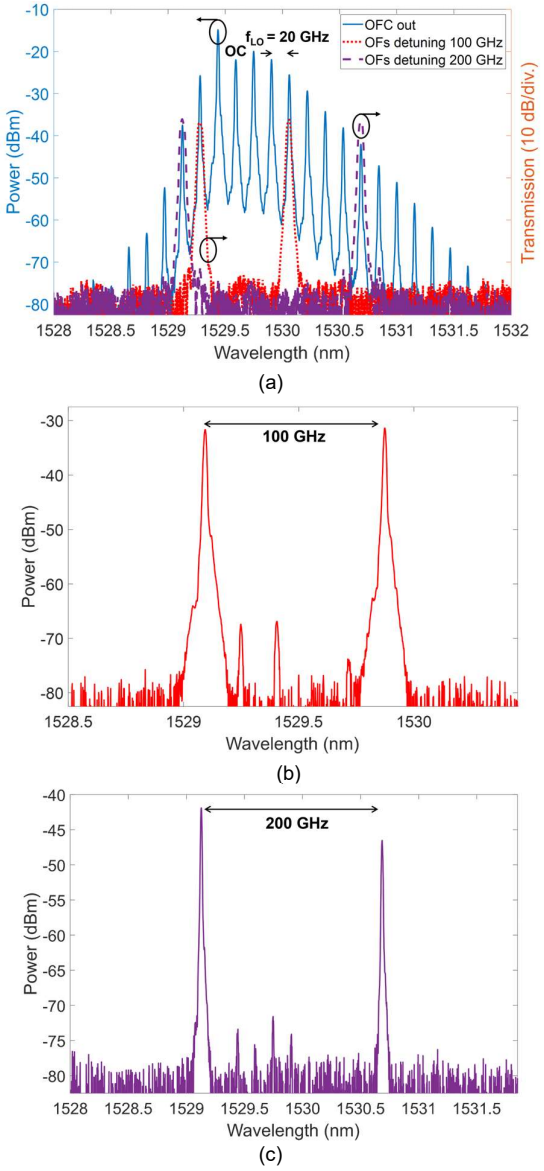

Fig. 5: (a) OFC signal (solid line) and OFs transmission spectra with relative detuning of 100 GHz (dotted line) and 200 GHz (dashed line) (OC: optical carrier). (b) PIC output spectrum for 100 GHz filter detuning; (c). (b) PIC output spectrum for 200 GHz filter detuning.

source driven by a LO at f_{LO} of 20 GHz, close to the 3 dB cut-off frequency of the modulator electro-optic response. The generated OFC spectrum when the LO power applied to the PM is ~1 W is shown in Fig. 5(a), along with the transmission shapes of the OFs for two relative detunig settings of 100 GHz and 200 GHz. The PIC output spectrum when the filters are tuned for selecting the 2nd-order shorter-wavelength and 3rd-order longer-wavelength 100 GHz-spaced harmonics of the comb (location of the original optical carrier is also indicated in Fig. 5(a)), is reported in Fig. 5(b). For this fivefold multiplication of the input 20 GHz LO frequency,

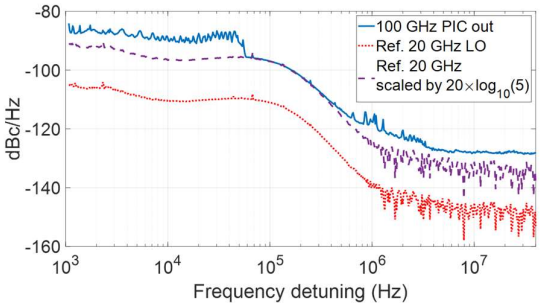

Fig. 6: Measured phase noise power spectral density of the generated 100 GHz RF carrier, of reference 20 GHz LO, and of corresponding ideal frequency multiplier.

a large rejection of the spurious tones of more than 35 dB is observed. When the OFs are tuned for selecting the 3rd-order shorter-wavelength and 7th-order longer-wavelength OFC harmonics, the minimum spurious tone rejection in the PIC output spectrum is 25 dB, limited in this case by the available spectral power of the selected 200-GHz spaced comb tones, as shown in Fig. 5(c).

Using a 100 GHz-bandwidth PD, the phase noise (PN) of the generated 100 GHz carrier wave is also characterized on a signal spectrum analyser. The results are shown in Fig. 6, where the power spectral densities of the reference LO PN and that of an ideal frequency multiplier (i.e., reference LO PN scaled by the square of the multiplication factor) are also reported. The discrepancy with the ideal frequency multiplier at low frequency is ascribed to low frequency fluctuations of the filters' central frequency, that can be mitigated by improving the quality of the control signals. The overall time jitter of the 100 GHz generated clock is 25 fs, whereas that of the reference 20 GHz signal is 17 fs.

Conclusions

We reported of a photonic integrated circuit in silicon on insulator technology for millimeter-wave band carrier wave synthesis. Using a simple single modulator-based comb source driven by a 20 GHz reference signal, up to 200 GHz spaced isolated optical tones have been generated at the circuit output. Improved operation is expected using a second on-chip cascaded modulators-based comb source.

Acknowledgements

This work was partially supported by the EU under the Italian National Recovery and Resilience Plan (NRRP) of NextGenerationEU, partnership on "Telecommunications of the Future" (PE00000001 - program "RESTART"), and by the Italian Ministry of University and Research through the COSMOS project (grant number FISR2019_0347).

References

[1] M. Xiao, S. Mumtaz, Y. Huang, L. Dai, Y. Li, M. Matthaiou, G.K. Karagiannidis, E. Björnson, K. Yang, I. Chih-Lin, and A. Ghosh, "Millimeter wave communications for future mobile networks. IEEE Journal on Selected Areas in Communications, vol. 35, no. 9, pp.1909-1935, 2017,
DOI: 10.1109/JSAC.2017.2719924

[2] Y. Niu, Y. Li, D. Jin, L. Su, and A. V. Vasilakos. "A survey of millimeter wave communications (mmWave) for 5G: opportunities and challenges." Wireless Networks, vol. 21, pp. 2657-2676, 2015,
DOI: 10.1007/s11276-015-0942-z

[3] K. V. Mishra, M. B. Shankar, V. Koivunen, B. Ottersten, and S. A. Vorobyov, "Toward millimeter-wave joint radar communications: A signal processing perspective". IEEE Signal Processing Magazine, vol. 36, no. 5, pp. 100-114, 2019,
DOI: 10.1109/MSP.2019.2913173

[4] D. M. Mittleman, "Twenty years of terahertz imaging [Invited]," Optics Express, vol. 26, no. 8, pp. 9417-9431 2018,
DOI: 10.1364/OE.26.009417

[5] A. Siligaris, Y. Andee, C. Jany, V. Puyal, J. M. Guerra, J.L.G. Jimenez, and P. Vincent, "A 270-to-300 GHz sub-harmonic injection locked oscillator for frequency synthesis in sub-mmW systems". IEEE Microwave and Wireless Components Letters, vol. 25, no. 4, pp.259-261, 2015.
DOI: 10.1109/LMWC.2015.2401980

[6] A. J. Seeds, H. Shams, M. J. Fice, and C. C. Renaud: Terahertz photonics for wireless communications, Journal of Lightwave Technology, vol. 33, no. 3, pp. 579–587, 2015,
DOI: 10.1109/JLT.2014.2355137

[7] A. Delmade, C. Browning, T. Verolet, J. Poette, A. Farhang, H. H. Elwan, R. D. Koilpillai, G. Aubin, F. Lelarge, A. Ramdane, D. Venkitesh, and L. P. Barry, "Optical heterodyne analog radio-over-fiber link for millimeter-wave wireless systems", Journal of Lightwave Technology, vol. 39, no. 2, pp. 465-474, 2020,
DOI: 10.1109/JLT.2020.3032923

[8] P.T. Dat, Y. Yamaguchi, M. Motoya, S. Oikawa, J. Ichikawa, A. Kanno, N. Yamamoto, and T. Kawanishi, Transparent Fiber–Millimeter-Wave–Fiber System in 100-GHz Band Using Optical Modulator and Photonic Down-Conversion, Journal of Lightwave Technology, vol. 40, no. 5, pp. 1483-1493, 2022,
DOI: 10.1109/JLT.2022.3141058

[9] K. Sengupta, T. Nagatsuma, and D. M. Mittleman, "Terahertz integrated electronic and hybrid electronic–photonic systems", Nature Electronics, vol. 1, no. 12, pp.622-635, 2018,
DOI: 10.1038/s41928-018-0173-2

[10] R. Guzmán, L. González, A. Zarzuelo, J. Cesar Cuello, M. Ali, I. Visscher, R. Grootjans, J. P. Epping, C.G. H. Roeloffzen, and G. Carpintero, "Widely Tunable RF Signal Generation Using an InP/Si_3N_4 Hybrid Integrated Dual-Wavelength Optical Heterodyne Source", Journal of Lightwave Technology, vol. 39, no. 24, pp. 7664-7671, 2021,
DOI: 10.1109/JLT.2021.3078508

[11] C. Porzi, F. Falconi, M. Sorel, P. Ghelfi, and A. Bogoni, "Flexible millimeter-wave carrier generation up to the Sub-THz with silicon photonics filters", Journal of Lightwave Technology, vol. 39, no. 24, pp. 7689-7697, 2021.
DOI: 10.1109/JLT.2021.3113896

[12] A. Malacarne, A. Bigongiari, A. D'Errico A. Bogoni, and C. Porzi, "Reconfigurable Low Phase Noise RF Carrier Generation up to W-Band in Silicon Photonics Technology", Journal of Lightwave Technology, vol. 40, no. 20, pp. 6891-900, 2022,
DOI: 10.1109/JLT.2022.3194361

[13] https://europractice-ic.com/technologies/photonics/imec/

[14] C. Porzi, G. J. Sharp, M. Sorel, and A. Bogoni, "Silicon photonics high-order distributed feedback resonators filters", Journal of Quantum Electronics, 56(1), pp.1-9, 2029.
DOI: 10.1109/JQE.2019.2960560